Sea Surface Salinity Provides Subseasonal Predictability for Forecasts of Opportunity of U.S. Summertime Precipitation

Marybeth Arcodia[1], Elizabeth A. Barnes[1], Paul James Durack[2], Patrick Keys[3], and Juliette Rocha[4]

[1]Colorado State University
[2]Lawrence Livermore National Laboratory (DOE)
[3]Department of Atmospheric Science, Colorado State University
[4]Texas A&M University

January 23, 2024

Abstract

As oceanic moisture evaporates, it leaves a signature on sea surface salinity. Roughly 10% of the moisture that evaporates over the ocean is transported over land, allowing the salinity fields to be a predictor of terrestrial precipitation. This research is among the first in published literature to assess the role of sea surface salinity for improved predictions on low-skill summertime subseasonal timescales for terrestrial precipitation predictions. Neural networks are trained with the CESM2 Large Ensemble using North Atlantic salinity anomalies to quantify predictability of U.S. Midwest summertime heavy rainfall events at 0 to 56-day leads. Using explainable artificial intelligence, salinity anomalies in the Caribbean Sea and Gulf of Mexico are found to provide skill for subseasonal forecasts of opportunity, e.g. confident and correct predictions. Further, a moisture-tracking algorithm applied to reanalysis data demonstrates that the regions of evaporation identified by neural networks directly provide moisture that precipitates in the Midwest.

Hosted file

984624_0_art_file_11783280_s7d5lp.docx available at https://authorea.com/users/541956/articles/701151-sea-surface-salinity-provides-subseasonal-predictability-for-forecasts-of-opportunity-of-u-s-summertime-precipitation

Sea Surface Salinity Provides Subseasonal Predictability for Forecasts of Opportunity of U.S. Summertime Precipitation

Marybeth C. Arcodia[1], Elizabeth A. Barnes[1], Paul J. Durack[2], Patrick W. Keys[1], Juliette Rocha[3]

[1]Department of Atmospheric Science, Colorado State University, Fort Collins, CO, USA.

[2]Program for Climate Model Diagnosis and Intercomparison (PCMDI), Lawrence Livermore National Laboratory, Livermore, CA, USA.

[3] Department of Atmospheric Science, Texas A&M University, College Station, TX, USA.

Corresponding author: Marybeth C. Arcodia (marcodia@rams.colostate.edu)

Key Points:

- Sea surface salinity anomalies provide predictability for heavy summertime Midwest precipitation events
- Subseasonal forecasts of opportunity for heavy precipitation are informed by positive salinity anomalies in the Caribbean and Gulf of Mexico
- Regions of evaporation identified by neural networks provide a direct moisture source for precipitation in the Midwest region

Abstract

As oceanic moisture evaporates, it leaves a signature on sea surface salinity. Roughly 10% of the moisture that evaporates over the ocean is transported over land, allowing the salinity fields to be a predictor of terrestrial precipitation. This research is among the first in published literature to assess the role of sea surface salinity for improved predictions on low-skill summertime subseasonal timescales for terrestrial precipitation predictions. Neural networks are trained with the CESM2 Large Ensemble using North Atlantic salinity anomalies to quantify predictability of U.S. Midwest summertime heavy rainfall events at 0 to 56-day leads. Using explainable artificial intelligence, salinity anomalies in the Caribbean Sea and Gulf of Mexico are found to provide skill for subseasonal forecasts of opportunity, e.g. confident and correct predictions. Further, a moisture-tracking algorithm applied to reanalysis data demonstrates that the regions of evaporation identified by neural networks directly provide moisture that precipitates in the Midwest.

Plain Language Summary

Global water cycling plays a fundamental role in the climate system, directly impacting terrestrial water availability. Roughly 10% of the moisture that evaporates over the ocean is transported over land, eventually falling as precipitation. As moisture evaporates from the ocean, the waters below become saltier, leaving an imprint on the sea surface salinity pattern. These salinity signatures can potentially be used as a predictor of landfalling precipitation in the coming weeks. This study uses neural networks to quantify the predictability of summertime precipitation in the Midwest from 0 to 56 days in advance using salinity patterns in the North Atlantic. High salinity in the Caribbean Sea and Gulf of Mexico is found to provide skill for subseasonal forecasts of opportunity, e.g. confident and correct predictions at 21-day leads. A moisture-tracking model traces the origin of water that falls as precipitation and confirms the Caribbean Sea and Gulf of Mexico as direct moisture sources for Midwest precipitation.

1 Introduction

Global water cycling plays a fundamental role in the climate system, directly impacting terrestrial water availability. The hydrological cycle consists of moisture evaporation in one location which falls as precipitation in another location via a balance of atmospheric, oceanic, and terrestrial water transport (Adler et al., 2003; Gimeno et al., 2010). The majority of moisture (~90%) that evaporates over the ocean rains out over the ocean (Trenberth et al., 2007). However, the remaining 10% of the moisture evaporated is transported over land, eventually falling as terrestrial precipitation (Gimeno et al., 2012; Trenberth et al., 2011). Intense and persistent precipitation events over land cannot be sustained by local terrestrial moisture recycling alone (Brubaker et al., 1993; Dirmeyer et al., 2009; Koster et al., 2004; Trenberth, 1999), highlighting ocean-derived moisture as a source of extreme terrestrial precipitation events from.

Oceanic evaporation increasingly acts as a source of terrestrial precipitation due to anthropogenic climate change (Gimeno et al., 2020). Rising atmospheric temperatures have led to more rapid evaporation over the oceans than over the land. This climate change response has intensified the oceanic water cycle (Durack et al., 2012), increasing the importance of oceanic evaporation for continental precipitation (Findell et al., 2019). As oceanic moisture evaporates it leaves a signature on sea surface salinity, allowing these fields to be a potential predictor of terrestrial precipitation (Schmitt, 2008).

Sea surface salinity has emerged as a potentially useful indicator of evaporation and subsequent moisture export from the ocean (Bengtsson, 2010). A close link exists between the oceanic water cycle and the sea surface salinity anomaly signal: positive anomalies (e.g. saltier waters) indicate evaporation of ocean waters and negative anomalies (e.g. fresher waters) indicate precipitation into the ocean (Durack, 2015). This relationship has led to an investigation into sea surface salinity as a potential seasonal predictor of terrestrial precipitation in the African Sahel (L. Li et al., 2016b), Southwestern U.S. (T. Liu et al., 2018), China (Zeng et al., 2019), and Australia (Rathore et al., 2020). In addition, Li et al. (2016a) and a followup study by Li et al. (2022) showed a strong relationship between springtime sea surface salinity in the northwestern subtropical North Atlantic and summertime precipitation in the U.S. Midwest, revealing sea surface salinity as a skillful *seasonal* predictor of U.S. Midwest summertime rainfall.

Here, we explore the predictability provided by North Atlantic sea surface salinity for *subseasonal* prediction of summertime U.S. Midwest precipitation. Subseasonal prediction (e.g. 2 weeks to one season ahead) bridges the gap between weather and climate (Lang et al., 2020) and supports sufficient lead time for storm and flood preparedness and informed resource management (DeFlorio et al., 2021). Heavy Midwest rainfall events in the summertime are particularly challenging to predict (L. Li et al., 2022; Z. Li & O'Gorman, 2020), yet the damage from these events can be extensive (Trenberth & Guillemot, 1996). For example, historic flooding throughout the Midwest region in spring-summer of 2013, dubbed a 500-year flooding event by a U.S. Geological Survey press release, resulted in over 10 fatalities and $400 million damages. Given the difficult predictive nature of summertime heavy rainfall events, we focus on identifying "forecasts of opportunity", e.g. predictions with high skill and confidence due to a predictable state of the climate system (Mariotti et al., 2020), and pinpointing their sources of predictability. To connect the climate model analysis to real-world dynamics, we employ a moisture tracking algorithm to determine the North Atlantic sources of evaporation that eventually fall in the Midwest as heavy precipitation events. This study reveals sea surface salinity as an effective subseasonal predictor for forecasts of opportunity of summertime Midwest heavy precipitation events.

2 Data and Methods

2.1 Climate Model Data Preprocessing

Artificial neural networks are trained to ingest maps of sea surface salinity anomaly maps to classify precipitation events into light or heavy precipitation events over the U.S. Midwest at leads of 0-56 days. Training neural networks requires a large amount of data (Adi et al., 2020), but observed daily sea surface salinity fields are not readily available in a usable (e.g. gridded) format (H. Wang et al., 2022). The few reanalysis datasets that provide daily sea surface salinity fields either do not cover the North Atlantic region needed for this study (e.g. the Global Tropical Moored Buoy Array) or do not have a long enough time series for adequate training (e.g. only ~30 years are provided by the Global Ocean Forecasting System HYCOM, which is insufficient for training in this study). Therefore, we take advantage of the long-running daily, gridded data from the Community Earth System Model Version 2- Large Ensemble (CESM2-LE; Danabasoglu et al., 2020) for analysis of 1,000 years of climate model data.

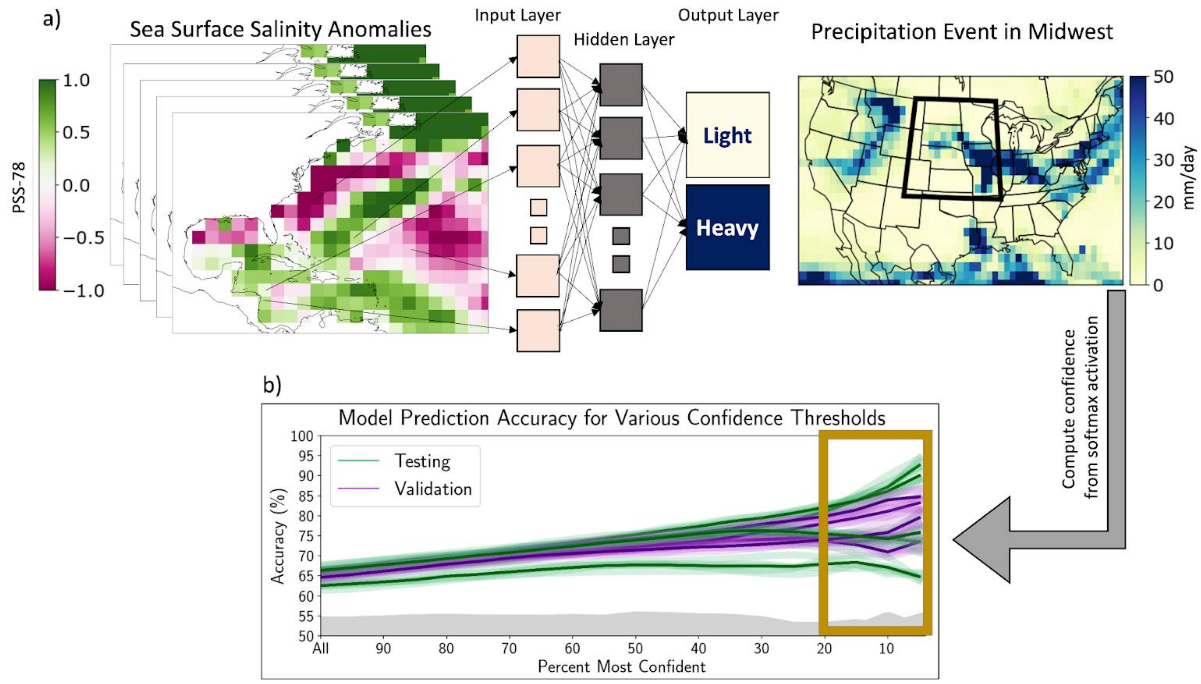

Figure 1. a) Schematic of the neural network architecture used in this study for a 21-day lead. b) The accuracy vs. confidence for 5 testing (green) and validation (purple) members using 5 random seeds each (light lines; dark lines represent the average) for 21-day lead predictions. Confidence is computed using the softmax activation on the output layer of the network in (a). A random network is represented with the gray shading. The gold box highlights the 20% most confident predictions.

We use 1850-1949 historical daily data from 10 CESM2 ensemble members, in which each ensemble member is considered to be an independent realization of the historical climate (Rodgers et al., 2021). Sea surface salinity fields in units based on the Practical Salinity Scale 1978 (PSS-78) span May-August to capture the U.S. Midwest summer. Daily anomalies are computed via subtraction of the linear trend at each grid point of the ensemble mean for each calendar-day of the year to remove the forced response, then smoothed with a 3-day running mean. Sea surface salinity anomalies span the North Atlantic region from 8N - 50N, 265E - 320E, including the Gulf of Mexico, but excluding all data from the Pacific (Fig. 1a left).

We use raw precipitation fields (e.g. not anomalies) of a 3-day cumulative sum averaged over the Midwest region- defined as 36N - 49N, 254E - 270E (Fig. 1a right). A Poisson weighting strategy (Fig. S1) adapted from Ford et al. (2018) is applied to the precipitation time series to smooth data as lead time increases for a seamless transition across timescales assessed (Hoskins, 2013). This technique broadens the event window to shift from deterministic to probabilistic forecasts and account for uncertainty as lead time increases (Fig. S1) (Dirmeyer et al., 2018; Dirmeyer & Ford, 2020; Ford et al., 2018). Once smoothed, periods above the 80th percentile of precipitation are classified as heavy events, designated as a 1, and the remaining 80% of the data classified as light events, designated as a 0.

2.2 Neural Network Setup

The feedforward artificial neural network approach consists of a 3-layer neural network: the input layer (3-day averaged sea surface salinity anomaly maps), 1 hidden layer, and the output layer (classification of light or heavy precipitation event in the Midwest boxed region). Neural networks are trained separately for each lead time. Additional details on data pre-processing and hyperparameter tuning are found in S1-2 and Tables S1-2.

2.3 Quantifying Forecasts of Opportunity

The final network output layer consists of the two nodes of our binary classification setup (Fig. 1a). The softmax activation function is applied to the final layer, transforming the two outputs to values which sum to 1, representing a probability estimate. This probability is used to select the predicted output in that the value which exceeds 0.5 is selected as the prediction. We leverage this output probability as our network confidence (Arcodia et al., 2023; Mayer & Barnes, 2021, 2022), allowing quantification of the prediction confidence. As confidence increases, accuracy also increases, suggesting that the network identifies intermittent patterns in the input salinity maps that lead it to be more confident in its prediction (Fig. 1b). Hereafter, we define the 20% most confident predictions, which are also found to be the most accurate predictions, as *forecasts of opportunity* (Fig. 1b; gold box).

2.4 Water Accounting Model

We employ the Water Accounting Model 2-layers (WAM2layers, version 3.0.0), a Eulerian moisture-tracking model that can trace the path of water from its origin as evaporation, through the atmosphere as water vapor, and to its eventual fate as precipitation elsewhere (van der Ent et al. 2014; van der Ent et al. 2023). The model uses European Centre for Medium-Range Weather Forecasts v5 (ERA5; Hersbach et al. 2020) climate reanalysis data to verify that the oceanic evaporative moisture source regions identified by the neural networks provide the moisture to Midwest precipitation events in the real world. Additional WAM2layers model details are found in S3.

3 Results

3.1 Subseasonal Forecasts of Opportunity

Accuracy for all summertime Midwest precipitation predictions shows the highest skill at leads 14- and 21-days (Fig. 2; blue squares). For the forecasts of opportunity, e.g. the 20% most confident predictions, accuracy peaks at lead 21-days (Fig. 2; gold diamonds), demonstrating that sea surface salinity anomalies serve as a meaningful predictor on subseasonal timescales. Notably, leads 7- through 21-days reveal accuracy above 75% on average for forecasts of opportunity for precipitation event prediction. Skill drops quickly to that of random chance for leads of 35-days and beyond (Fig. 2; gray shading).

Fig. 2a shows accuracies for balanced test data (see S1), meaning the likelihood of a heavy precipitation event is 50%. However, based on the definition of a heavy event (>80th percentile), the true likelihood of a heavy event is 20%. We use two skill scores: 1. Threat Score (Fig. 2b) and 2. Gilbert Skill Score (Fig. 2c); see S4 for definitions. These scores are verification metrics of forecasts in which a score of zero denotes no skill, or random chance, and a skill of one is a perfect score. Skill scores are used to evaluate the performance of the networks on unbalanced data to determine if network prediction skill is due to accurate predictions of both classes, or if the network has learned only the majority class. The variation in skill as a function of lead time follows a similar pattern for the balanced and unbalanced datasets, with a peak in skill at subseasonal lead time of 21 days, particularly for forecasts of opportunity. Networks have learned patterns within the data to not only predict light but also heavy events, demonstrating the utility of sea surface salinity as a predictor for high-impact heavy precipitation events.

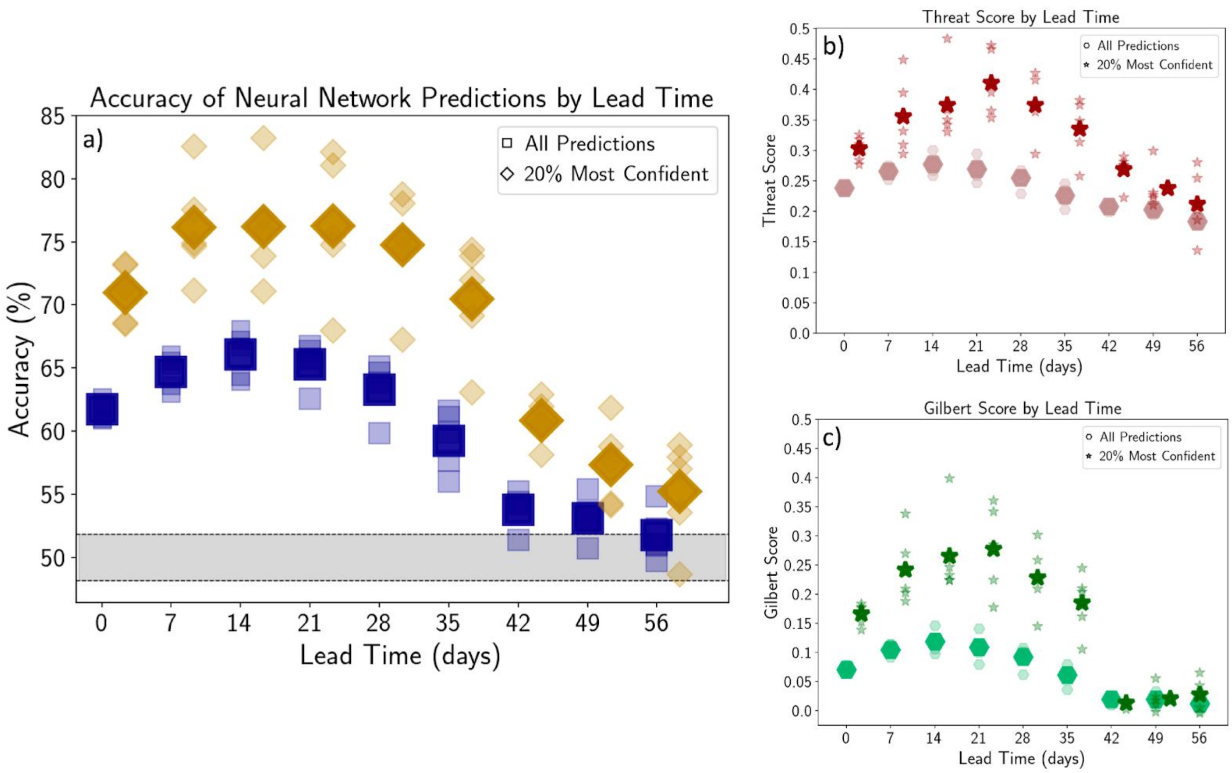

Figure 2. a) Accuracy as a function of lead time in days for all predictions (blue squares) and forecasts of opportunity (gold diamonds). The lightly shaded shapes represent the averaged accuracy from five random seeds for each test ensemble member with balanced data, and the darker, larger shapes represent the average accuracy from all 5 test ensemble members. The gray shading denotes the 99% confidence intervals of a binomial probability (e.g. random chance). b) The Threat Score as a function of lead time computed on predictions with unbalanced data for all predictions (hexagons) and forecasts of opportunity (stars). c) Same as b) but for the Gilbert Skill Score. For (b) and (c), a score of zero denotes no skill, or random chance, and a skill of one is a perfect score.

After determining that the networks can result in skillful and confident predictions on subseasonal lead time times, we want to know *why* the network made these predictions. We find that for skillful forecasts of opportunity for heavy precipitation, sea surface salinity anomalies in the Caribbean Sea and Gulf of Mexico are predominantly positive (Fig. 3a). That is, saltier waters in these regions imply evaporation and atmospheric moisture available for transportation out of the region. Conversely, for skillful light precipitation predictions, we find negative sea surface salinity anomalies, indicating precipitation (Fig. 3b). This pattern reflects less atmospheric moisture from the oceanic source region available to be transported away, resulting in a confident subseasonal predictions of no heavy rainfall event.

We complement the salinity composite maps associated with forecasts of opportunity with *explainable artificial intelligence* (XAI) to pinpoint regions that the network deems as important in making its prediction (e.g. Arcodia et al., 2023; Mamalakis, Barnes, et al., 2022;

Mayer & Barnes, 2021; McGovern et al., 2019; Pegion et al., 2022; Rader et al., 2022). Here, the *gradient* method is applied to compute the gradient of the network output with respect to the input grid points to visualize the sensitivity of the networks to the salinity anomalies at lead 21-days (Mamalakis, Ebert-Uphoff, et al., 2022) (Fig. 3c; composites and heatmaps for all leads in Figs. S3 and S4). For correct and confident heavy predictions, the sensitivity of the network to changes in salinity anomalies is most prominent in the Caribbean Sea and Gulf of Mexico. Saltier waters in these regions are found to increase confidence in heavy predictions. Regions with near-zero salinity anomalies south of Jamaica and negative salinity anomalies along the East Coast in the Gulf Stream region decrease confidence in heavy predictions. That is, network confidence for heavy subseasonal predictions strengthens as water becomes saltier in the Caribbean and Gulf of Mexico. Thus, anomalously salty waters in the Caribbean and Gulf of Mexico provide predictability for heavy precipitation events in the U.S. Midwest on subseasonal timescales.

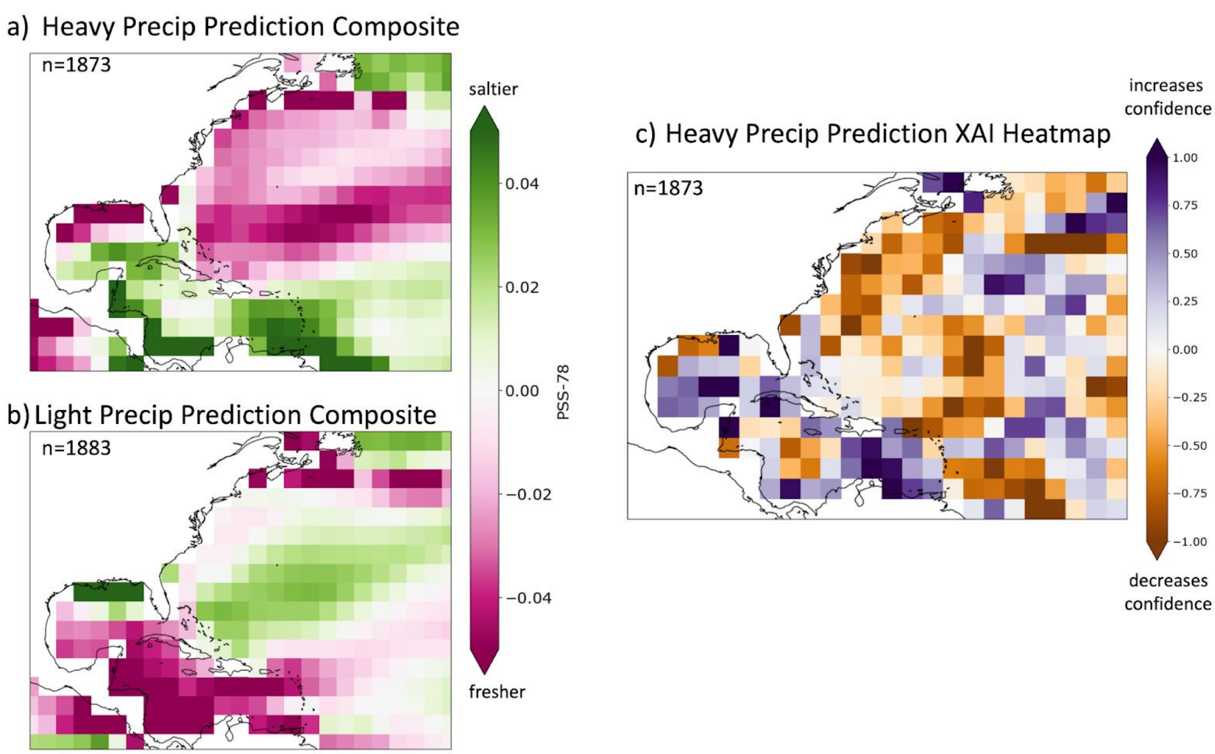

Figure 3. a-b) Composite of the sea surface salinity anomalies in PSS-78 for input maps of the 20% most confident, correct predictions for a 21-day lead for heavy predictions (a) and light predictions (b). Composites use input from each test ensemble member from the neural network initialized with the random seed that results in the highest accuracy. c) Saliency XAI composited heatmaps for the same days as the input maps as (a). The colorbar is a unitless measure of sensitivity. The number *n* represents the number of samples per composite.

3.2 Moisture Tracking with ERA5

The neural networks used thus far were trained, validated, and tested on 1,000 collective years of CESM2 historical climate model data. Unfortunately, like all climate models, CESM2 exhibits biases which can result in limitations for its use for understanding the real world (Simpson et al., 2020). Therefore, we employ the WAM2layers model and present-day reanalysis data (van der Ent et al. 2023) to track where evaporation occurred, which would later fall as precipitation in a specific region. We track moisture within ERA5 using the WAM2layers model for May-August (MJJA) from 2008-2021 to pinpoint the origin of all moisture which eventually falls in the Midwest region (Fig. 4a). The majority of Midwest moisture is found to be locally recycled, consistent with Bosilovich and Schubert (2002) who showed the largest source of precipitation in the midwestern U.S. came from local moisture recycling. However, we also find that summertime Midwest precipitation has an *oceanic* moisture source in the Gulf of Mexico and the Caribbean Sea regions without recycling, consistent with the regions of sea surface salinity anomalies identified by the neural networks as relevant for forecasts of opportunity (Fig. 3).

Another primary moisture source region for the Midwest is the area directly to the south (Fig. 4a), indicating that the southern U.S. acts as an additional moisture source region. The WAM2layers results for moisture-tracking of the southern U.S. also highlight the Gulf of Mexico and Caribbean Sea (Fig. 4b). Moisture which evaporates over the Gulf of Mexico and Caribbean Sea likely acts as a moisture source for Midwest precipitation in 2 ways: 1) moisture is directly transported and precipitates in the Midwest, or 2) moisture falls as precipitation in the southern U.S. region which is then locally recycled and transported north to eventually precipitate in the Midwest. Thus, the networks have identified physically meaningful sources of predictability, consistent with the patterns found in the composite and XAI maps (Fig. 3), which can ultimately provide subseasonal prediction skill for U.S. Midwest heavy rainfall events.

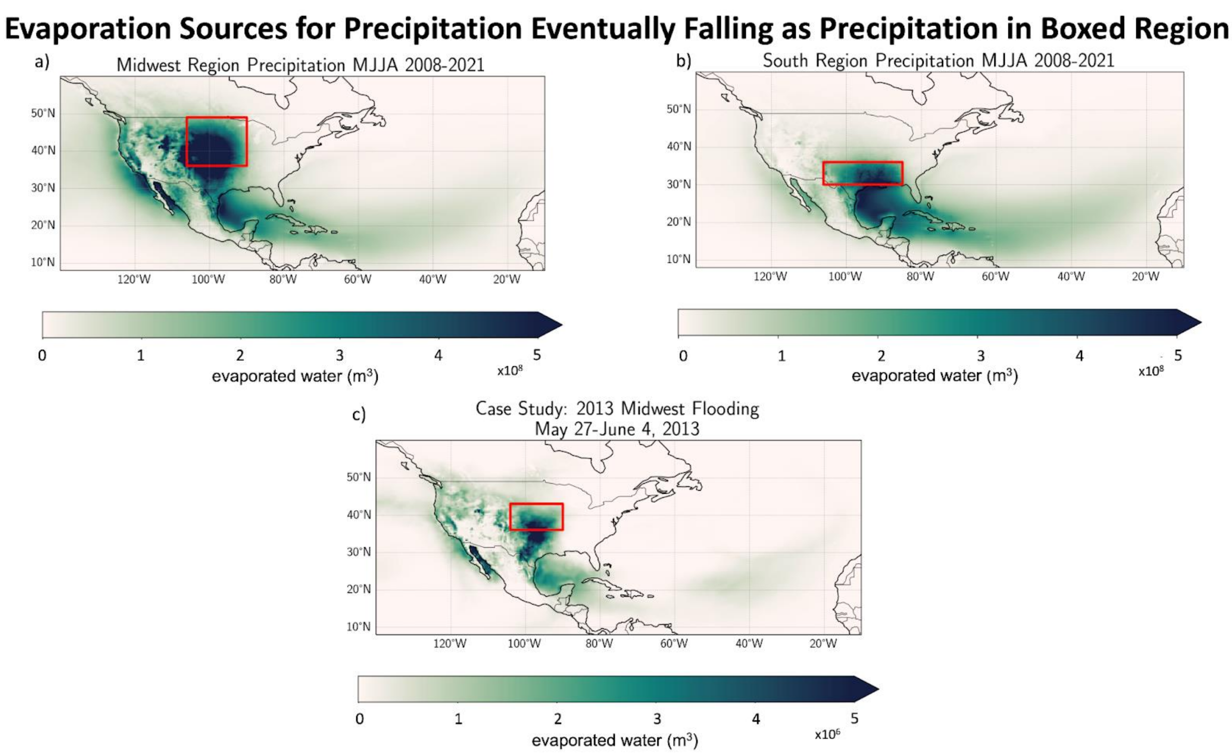

Figure 4. The sum of the evaporated water (in cubic meters) which fell as precipitation in the red boxed regions computed using the WAM2layers backtracking algorithm for the Midwest (a) and South U.S. region (b) for May-August from 2008-2021. c) shows the same, but for the southern Midwest region (red box) for May 27-June 4, 2013.

Lastly, we analyze a case study to verify the Gulf of Mexico and Caribbean Sea can provide moisture sources for specific heavy precipitation events in the Midwest. We analyze a 9-day period of intense rainfall in the Midwest region from May 27 - June 4, 2013 when over 150 mm of rainfall was recorded in the Missouri and southeastern Midwest areas (USGS, 2013) (Fig. 4c). We find that the local region (red box), southern U.S., and Gulf of Mexico/ Caribbean Sea are the largest moisture source regions for the observed extreme precipitation. Approximately 22% of the moisture originated from the Caribbean Sea and Gulf of Mexico region and was directly transported and precipitated in the Midwest during this event (see S5 and Fig. S4), while only 11% of the moisture was locally recycled. An additional case study is shown in Supplemental Fig. 5 for the 2011 Missouri River Flooding events from May-June in which approximately 21% directly originated from the Caribbean and Gulf of Mexico region and 14% of the moisture was locally recycled.

The results from the WAM2layers water tracking model reveal that evaporation over the Gulf of Mexico and Caribbean Sea acts as a moisture source for precipitation over the Midwest in summertime. These results support our findings that evaporation in these regions indicated by sea surface salinity anomalies can provide predictive skill for heavy summertime Midwest precipitation events.

4 Discussion

This analysis has revealed that salty waters indicative of evaporation in the Caribbean and Gulf of Mexico (Fig. 3) provide predictability for subseasonal forecasts of opportunity for heavy Midwest precipitation events (Fig. 2). We discuss a potential physical link for how the evaporative moisture source regions, identified by neural networks, provide moisture that ultimately precipitates in the Midwest region. The Caribbean Sea has been documented to provide significant moisture sources for Midwest extreme precipitation events via dynamical links from low-level jets (Dirmeyer & Kinter, 2010). In the summertime, a branch of the Caribbean Low-level Jet (CLLJ) turns northward and connects with the Great Plain Low-level Jet (GPLLJ) (Amador, 1998; Cook & Vizy, 2010). This causes a shift in westward moisture transport over the Caribbean Sea to northward transport over the continental U.S. into the Great Plains and Midwest regions (C. Wang et al., 2007). The interactions of these jets are intimately tied to the North Atlantic Subtropical High (NASH), a robust atmospheric high pressure in the North Atlantic region which impacts the strength and location of the low-level jets and their surface evaporation (C. Wang et al., 2007). The lower branch of the NASH is reflected in the swooping evaporated water feature found from the WAM2layers analysis in Fig. 4, supporting the dynamical link between subtropical jet features and Midwest precipitation. Putting it all together, evaporation in the Caribbean and Gulf of Mexico increases atmospheric moisture availability which is then transported westward by the Caribbean Low-level Jet and northward into continental U.S. and Midwest by the Great Plains Low-level jet.

Li et al. (2018) showed that a soil moisture feedback mechanism connects North Atlantic sea surface salinity anomalies to Midwest summertime precipitation. Enhanced moisture export from the subtropical North Atlantic contributes to extreme rainfall in the southern U.S. leading to increased soil moisture. This soil moisture feedback causes enhanced evaporation and atmospheric convection, which intensifies the GPLLJ and transports moisture to the Midwest region. Additional research into the prediction of the location and intensity of these jets and the NASH (e.g. Ferguson, 2022; García-Martínez & Bollasina, 2020; Krishnamurthy et al., 2015; Malloy & Kirtman, 2020) could provide added predictive skill for forecasts of opportunity for Midwest precipitation events.

Sea surface salinity biases have been documented in CESM2 linked to precipitation biases (Simpson et al., 2020; Wei et al., 2021) with a slightly fresh overall salinity bias (Y. Liu et al., 2022). There are also discrepancies between satellite and in-situ sea surface salinity data due to both observational and sampling errors which provide constraints for ocean models (Vinogradova et al., 2019). Further, CESM2 sea surface salinity data is taken as the average of the upper 10m of the ocean. Boutin et al. (2016) show that near-surface stratification of salinity exists in the upper 1m and subseasonal prediction could vary based on this upper ocean resolution (Subramanian et al., 2019). We note that the predictive skill of heavy precipitation events using higher vertical resolution sea surface salinity data may vary as this could more effectively capture skin-layer evaporation intensity, rather than muted anomalies represented in the 0-10m volume average, but we leave this investigation for future work.

5 Conclusions

This study is the first peer-reviewed documentation to demonstrate the utility of North Atlantic sea surface salinity anomalies as a skillful subseasonal predictor of heavy Midwest summertime precipitation events. We employ a machine learning approach using neural networks to quantify the subseasonal predictability of heavy summertime rainfall events in the U.S. Midwest region using 3-day North Atlantic sea surface salinity fields. Using a statistical smoothing for a seamless transition across timescales, we assess predictability for lead times from 0-days to 56-days. We find that predictive skill is highest on subseasonal timescales with a peak at 21-day lead, particularly for forecasts of opportunity, e.g. predictions which are both confident and accurate. Output from neural networks allows us to identify predictions which result in forecasts of opportunity. Using explainable artificial intelligence, we create heatmaps of the most sensitive regions of salinity anomalies in the tropical and North Atlantic which provide skill for forecasts of opportunity. Positive sea surface salinity anomalies (which indicate evaporation and increased atmospheric moisture availability) in the Caribbean and Gulf of Mexico provide predictability for the forecasts of opportunity for heavy precipitation events. Consistent with previous research highlighting subtropical North Atlantic moisture as a source of U.S. terrestrial precipitation (Gimeno et al., 2010; L. Li et al., 2016a, 2022; van der Ent et al., 2010), our results support a physically consistent link between evaporation in the Caribbean and Gulf of Mexico and heavy precipitation in the Midwest via low-level jets. Output from the WAM2layers moisture-tracking model reveals that the regions of evaporation identified by neural networks within CESM2 simulations provide moisture to the Midwest region in the ERA5 atmospheric reanalysis. The Caribbean Sea and Gulf of Mexico are found to provide a direct oceanic moisture source for Midwest precipitation, in part without moisture recycling, linking the salinity anomalies to subseasonal predictive skill of Midwest precipitation. These results complement the explainable artificial intelligence findings to reveal robust and physically meaningful sources of summertime heavy Midwest precipitation predictability via Atlantic sea surface salinity anomalies.

Acknowledgments

This study was performed as part of the Program for Climate Model Diagnosis and Intercomparison (PCMDI), supported by the Regional and Global Modeling Analysis (RGMA) program area of U.S. DOE's Biological and Environmental Research (BER) Program. Work was performed under the auspices of the U.S. DOE by Lawrence Livermore National Laboratory under contract DEAC52-07NA27344. LLNL Release Number: LLNL-JNRL-859091. The authors declare no conflict of interest.

Open Research

CESM2 Large Ensemble Data are available freely to the public at www.cesm.ucar.edu/community-projects/lens2. The code for the Water Accounting Model 2-layers is available on GitHub, and is posted to the Zenodo permanent repository: https://doi.org/10.5281/zenodo.8172344. The ERA5 data were downloaded from the Copernicus Climate Data Store, and are freely available at https://cds.climate.copernicus.eu/cdsapp#!/dataset/reanalysis-era5-complete?tab=overview. All Python code for processing data and figures for this analysis will be available to the public on Github and converted to a permanent repository on Zenodo at the time of acceptance for publication.

References

Adi, E., Anwar, A., Baig, Z., & Zeadally, S. (2020). Machine learning and data analytics for the IoT. *Neural Computing & Applications*, *32*(20), 16205–16233.

Adler, R. F., Huffman, G. J., Chang, A., Ferraro, R., Xie, P.-P., Janowiak, J., Rudolf, B., Schneider, U., Curtis, S., Bolvin, D., Gruber, A., Susskind, J., Arkin, P., & Nelkin, E. (2003). The Version-2 Global Precipitation Climatology Project (GPCP) Monthly Precipitation Analysis (1979–Present). *Journal of Hydrometeorology*, *4*(6), 1147–1167.

Amador, J. A. (1998). A climate feature of the tropical Americas: The trade wind easterly jet. *Topicos Meteorologicos Oceanograficos*.

Arcodia, M. C., Barnes, E. A., Mayer, K. J., Lee, J., Ordonez, A., & Ahn, M.-S. (2023). Assessing decadal variability of subseasonal forecasts of opportunity using explainable AI. *Environmental Research: Climate*, *2*(4), 045002.

Bengtsson, L. (2010). The global atmospheric water cycle. *Environmental Research Lettters*, *5*(2), 025202.

Bosilovich, M. G., & Schubert, S. D. (2002). Water Vapor Tracers as Diagnostics of the Regional Hydrologic Cycle. *Journal of Hydrometeorology*, *3*(2), 149–165.

Boutin, J., Chao, Y., Asher, W. E., Delcroix, T., Drucker, R., Drushka, K., Kolodziejczyk, N., Lee, T., Reul, N., Reverdin, G., Schanze, J., Soloviev, A., Yu, L., Anderson, J., Brucker, L., Dinnat, E., Santos-Garcia, A., Jones, W. L., Maes, C., … Ward, B. (2016). Satellite and In Situ Salinity: Understanding Near-Surface Stratification and Subfootprint Variability. *Bulletin of the American Meteorological Society*, *97*(8), 1391–1407.

Brubaker, K. L., Entekhabi, D., & Eagleson, P. S. (1993). Estimation of Continental Precipitation Recycling. *Journal of Climate*, *6*(6), 1077–1089.

Cook, K. H., & Vizy, E. K. (2010). Hydrodynamics of the Caribbean Low-Level Jet and Its Relationship to Precipitation. *Journal of Climate*, *23*(6), 1477–1494.

Danabasoglu, G., Lamarque, J.-F., Bacmeister, J., Bailey, D. A., DuVivier, A. K., Edwards, J., Emmons, L. K., Fasullo, J., Garcia, R., Gettelman, A., Hannay, C., Holland, M. M., Large, W. G., Lauritzen, P. H., Lawrence, D. M., Lenaerts, J. T. M., Lindsay, K., Lipscomb, W. H., Mills, M. J., … Strand, W. G. (2020). The community earth system model version 2 (CESM2). *Journal of Advances in Modeling Earth Systems*, *12*(2). https://doi.org/10.1029/2019ms001916

DeFlorio, M. J., Ralph, F. M., Waliser, D. E., Jones, J., & Anderson, M. L. (2021). *Better Subseasonal-to-Seasonal Forecasts for Water Management*. Eos, 102. https://doi.org/10.1029/2021EO159749

Dirmeyer, P. A., Adam Schlosser, C., & Brubaker, K. L. (2009). Precipitation, Recycling, and Land Memory: An Integrated Analysis. *Journal of Hydrometeorology*, *10*(1), 278–288.

Dirmeyer, P. A., & Ford, T. W. (2020). A Technique for Seamless Forecast Construction and Validation from Weather to Monthly Time Scales. *Monthly Weather Review*, *148*(9), 3589–3603.

Dirmeyer, P. A., Halder, S., & Bombardi, R. (2018). On the harvest of predictability from land states in a global forecast model. *Journal of Geophysical Research*, *123*(23), 13,111–113,127.

Dirmeyer, P. A., & Kinter, J. L. (2010). Floods over the U.S. Midwest: A Regional Water Cycle

Perspective. *Journal of Hydrometeorology*, *11*(5), 1172–1181.

Durack, P. J. (2015). Ocean Salinity and the Global Water Cycle. *Oceanography* , *28*(1), 20–31.

Durack, P. J., Wijffels, S. E., & Matear, R. J. (2012). Ocean salinities reveal strong global water cycle intensification during 1950 to 2000. *Science*, *336*(6080), 455–458.

Ferguson, C. R. (2022). Changes in great plains low-level jet structure and associated precipitation over the 20th century. *Journal of Geophysical Research*, *127*(3). https://doi.org/10.1029/2021jd035859

Findell, K. L., Keys, P. W., van der Ent, R. J., Lintner, B. R., Berg, A., & Krasting, J. P. (2019). Rising Temperatures Increase Importance of Oceanic Evaporation as a Source for Continental Precipitation. *Journal of Climate*, *32*(22), 7713–7726.

Ford, T. W., Dirmeyer, P. A., & Benson, D. O. (2018). Evaluation of heat wave forecasts seamlessly across subseasonal timescales. *Npj Climate and Atmospheric Science*, *1*(1), 1–9.

García-Martínez, I. M., & Bollasina, M. A. (2020). Sub-monthly evolution of the Caribbean Low-Level Jet and its relationship with regional precipitation and atmospheric circulation. *Climate Dynamics*, *54*(9), 4423–4440.

Gimeno, L., Drumond, A., Nieto, R., Trigo, R. M., & Stohl, A. (2010). On the origin of continental precipitation. *Geophysical Research Letters*, *37*(13). https://doi.org/10.1029/2010gl043712

Gimeno, L., Nieto, R., & Sorí, R. (2020). The growing importance of oceanic moisture sources for continental precipitation. *Npj Climate and Atmospheric Science*, *3*(1), 1–9.

Gimeno, L., Stohl, A., Trigo, R. M., Dominguez, F., Yoshimura, K., Yu, L., Drumond, A., Durán-Quesada, A. M., & Nieto, R. (2012). Oceanic and terrestrial sources of continental precipitation. *Reviews of Geophysics*, *50*(4). https://doi.org/10.1029/2012RG000389

Hersbach, H., Bell, B., Berrisford, P., Hirahara, S., Horányi, A., Muñoz-Sabater, J., Nicolas, J., Peubey, C., Radu, R., Schepers, D., Simmons, A., Soci, C., Abdalla, S., Abellan, X., Balsamo, G., Bechtold, P., Biavati, G., Bidlot, J., Bonavita, M., … Jean-Noël Thépaut. (2020). The ERA5 global reanalysis. *Quarterly Journal of the Royal Meteorological Society*, *146*(730), 1999–2049.

Hoskins, B. (2013). The potential for skill across the range of the seamless weather-climate prediction problem: a stimulus for our science. *Quarterly Journal of the Royal Meteorological Society*, *139*(672), 573–584.

Koster, R. D., Dirmeyer, P. A., Guo, Z., Bonan, G., Chan, E., Cox, P., Gordon, C. T., Kanae, S., Kowalczyk, E., Lawrence, D., Liu, P., Lu, C.-H., Malyshev, S., McAvaney, B., Mitchell, K., Mocko, D., Oki, T., Oleson, K., Pitman, A., … GLACE Team. (2004). Regions of strong coupling between soil moisture and precipitation. *Science*, *305*(5687), 1138–1140.

Krishnamurthy, L., Vecchi, G. A., Msadek, R., Wittenberg, A., Delworth, T. L., & Zeng, F. (2015). The Seasonality of the Great Plains Low-Level Jet and ENSO Relationship. *Journal of Climate*, *28*(11), 4525–4544.

Lang, A. L., Kathleen, Pegion, & Barnes, E. (2020). Introduction to special collection: “bridging weather and climate: Subseasonal-to-seasonal (S2S) prediction.” *Journal of Geophysical Research*, *125*(4). https://doi.org/10.1029/2019jd031833

Li, L., Schmitt, R. W., & Ummenhofer, C. C. (2018). The role of the subtropical North Atlantic water cycle in recent US extreme precipitation events. *Climate Dynamics*, *50*(3), 1291–1305.

Li, L., Schmitt, R. W., & Ummenhofer, C. C. (2022). Skillful long-lead prediction of summertime heavy rainfall in the US Midwest from sea surface salinity. *Geophysical Research Letters*, *49*(13). https://doi.org/10.1029/2022gl098554

Li, L., Schmitt, R. W., Ummenhofer, C. C., & Karnauskas, K. B. (2016a). Implications of North Atlantic Sea Surface Salinity for Summer Precipitation over the U.S. Midwest: Mechanisms and Predictive Value. *Journal of Climate*, *29*(9), 3143–3159.

Li, L., Schmitt, R. W., Ummenhofer, C. C., & Karnauskas, K. B. (2016b). North Atlantic salinity as a predictor of Sahel rainfall. *Science Advances*, *2*(5), e1501588.

Liu, T., Schmitt, R. W., & Li, L. (2018). Global Search for Autumn-Lead Sea Surface Salinity Predictors of Winter Precipitation in Southwestern United States. *Geophysical Research Letters*, *45*(16), 8445–8454.

Liu, Y., Cheng, L., Pan, Y., Tan, Z., Abraham, J., Zhang, B., Zhu, J., & Song, J. (2022). How Well Do

CMIP6 and CMIP5 Models Simulate the Climatological Seasonal Variations in Ocean Salinity? *Advances in Atmospheric Sciences*, *39*(10), 1650–1672.

Li, Z., & O'Gorman, P. A. (2020). Response of Vertical Velocities in Extratropical Precipitation Extremes to Climate Change. *Journal of Climate*, *33*(16), 7125–7139.

Malloy, K. M., & Kirtman, B. P. (2020). Predictability of Midsummer Great Plains Low-Level Jet and Associated Precipitation. *Weather and Forecasting*, *35*(1), 215–235.

Mamalakis, A., Barnes, E. A., & Ebert-Uphoff, I. (2022). Investigating the Fidelity of Explainable Artificial Intelligence Methods for Applications of Convolutional Neural Networks in Geoscience. *Artificial Intelligence for the Earth Systems*, *1*(4). https://doi.org/10.1175/AIES-D-22-0012.1

Mamalakis, A., Ebert-Uphoff, I., & Barnes, E. A. (2022). Neural network attribution methods for problems in geoscience: A novel synthetic benchmark dataset. *Environmental Data Science*, *1*, e8.

Mariotti, A., Baggett, C., Barnes, E. A., Becker, E., Butler, A., Collins, D. C., Dirmeyer, P. A., Ferranti, L., Johnson, N. C., Jones, J., Kirtman, B. P., Lang, A. L., Molod, A., Newman, M., Robertson, A. W., Schubert, S., Waliser, D. E., & Albers, J. (2020). Windows of Opportunity for Skillful Forecasts Subseasonal to Seasonal and Beyond. *Bulletin of the American Meteorological Society*, *101*(5), E608–E625.

Mayer, K. J., & Barnes, E. A. (2021). Subseasonal forecasts of opportunity identified by an explainable neural network. *Geophysical Research Letters*, *48*(10). https://doi.org/10.1029/2020gl092092

Mayer, K. J., & Barnes, E. A. (2022). Quantifying the effect of climate change on midlatitude subseasonal prediction skill provided by the tropics. *Geophysical Research Letters*, *49*(14). https://doi.org/10.1029/2022gl098663

McGovern, A., Lagerquist, R., Gagne, D. J., Eli Jergensen, G., Elmore, K. L., Homeyer, C. R., & Smith, T. (2019). Making the Black Box More Transparent: Understanding the Physical Implications of Machine Learning. *Bulletin of the American Meteorological Society*, *100*(11), 2175–2199.

O'Malley, T., Bursztein, E., Long, J., Chollet, F., Jin, H., Invernizzi, L., & Others. (2019). *KerasTuner*. https://github.com/keras-team/keras-tuner

Pegion, K., Becker, E. J., & Kirtman, B. P. (2022). Understanding Predictability of Daily Southeast U.S. Precipitation Using Explainable Machine Learning. *Artificial Intelligence for the Earth Systems*, *1*(4). https://doi.org/10.1175/AIES-D-22-0011.1

Rader, J. K., Barnes, E. A., Ebert-Uphoff, I., & Anderson, C. (2022). Detection of forced change within combined climate fields using explainable neural networks. *Journal of Advances in Modeling Earth Systems*, *14*(7). https://doi.org/10.1029/2021ms002941

Rathore, S., Bindoff, N. L., Ummenhofer, C. C., Phillips, H. E., & Feng, M. (2020). Near-Surface Salinity Reveals the Oceanic Sources of Moisture for Australian Precipitation through Atmospheric Moisture Transport. *Journal of Climate*, *33*(15), 6707–6730.

Rodgers, K. B., Lee, S.-S., Rosenbloom, N., Timmermann, A., Danabasoglu, G., Deser, C., Edwards, J., Kim, J.-E., Simpson, I. R., Stein, K., Stuecker, M. F., Yamaguchi, R., Bódai, T., Chung, E.-S., Huang, L., Kim, W. M., Lamarque, J.-F., Lombardozzi, D. L., Wieder, W. R., & Yeager, S. G. (2021). Ubiquity of human-induced changes in climate variability. *Earth System Dynamics*, *12*(4), 1393–1411.

Schmitt, R. (2008). Salinity and the global water cycle. *Oceanography*, *21*, 12–19.

Simpson, I. R., Bacmeister, J., Neale, R. B., Hannay, C., Gettelman, A., Garcia, R. R., Lauritzen, P. H., Marsh, D. R., Mills, M. J., Medeiros, B., & Richter, J. H. (2020). An evaluation of the large-scale atmospheric circulation and its variability in CESM2 and other CMIP models. *Journal of Geophysical Research*, *125*(13). https://doi.org/10.1029/2020jd032835

Subramanian, A. C., Balmaseda, M. A., Centurioni, L., Chattopadhyay, R., Cornuelle, B. D., DeMott, C., Flatau, M., Fujii, Y., Giglio, D., Gille, S. T., Hamill, T. M., Hendon, H., Hoteit, I., Kumar, A., Lee, J.-H., Lucas, A. J., Mahadevan, A., Matsueda, M., Nam, S., … Zhang, C. (2019). Ocean Observations to Improve Our Understanding, Modeling, and Forecasting of Subseasonal-to-Seasonal Variability. *Frontiers in Marine Science*, *6*. https://doi.org/10.3389/fmars.2019.00427

Trenberth, K. E. (1999). Atmospheric Moisture Recycling: Role of Advection and Local Evaporation. *Journal of Climate*, *12*(5), 1368–1381.

Trenberth, K. E., Fasullo, J. T., & Mackaro, J. (2011). Atmospheric Moisture Transports from Ocean to Land and Global Energy Flows in Reanalyses. *Journal of Climate*, *24*(18), 4907–4924.

Trenberth, K. E., & Guillemot, C. J. (1996). Physical Processes Involved in the 1988 Drought and 1993 Floods in North America. *Journal of Climate*, *9*(6), 1288–1298.

Trenberth, K. E., Smith, L., Qian, T., Dai, A., & Fasullo, J. (2007). Estimates of the Global Water Budget and Its Annual Cycle Using Observational and Model Data. *Journal of Hydrometeorology*, *8*(4), 758–769.

U.S. Geological Survey Office. (2013, June 3). *Friday Storms Caused Record Flooding on Fourche LaFave River in Scott and Yell Counties - U.S. Geological Survey Press release*. LegiStorm. https://www.legistorm.com/stormfeed/view_rss/278658/organization/35286/title/friday-storms-caused-record-flooding-on-fourche-lafave-river-in-scott-and-yell-counties.html

USGS. (2013). *May-June 2013 Midwest Floods*. https://www.usgs.gov/mission-areas/water-resources/science/may-june-2013-midwest-floods

van der Ent, R. J., Savenije, H. H. G., Schaefli, B., & Steele-Dunne, S. C. (2010). Origin and fate of atmospheric moisture over continents. *Water Resources Research*, *46*(9). https://doi.org/10.1029/2010wr009127

Vinogradova, N., Lee, T., Boutin, J., Drushka, K., Fournier, S., Sabia, R., Stammer, D., Bayler, E., Reul, N., Gordon, A., Melnichenko, O., Li, L., Hackert, E., Martin, M., Kolodziejczyk, N., Hasson, A., Brown, S., Misra, S., & Lindstrom, E. (2019). Satellite Salinity Observing System: Recent Discoveries and the Way Forward. *Frontiers in Marine Science*, *6*. https://doi.org/10.3389/fmars.2019.00243

Wang, C., Lee, S.-K., & Enfield, D. B. (2007). Impact of the Atlantic Warm Pool on the Summer Climate of the Western Hemisphere. *Journal of Climate*, *20*(20), 5021–5040.

Wang, H., You, Z., Guo, H., Zhang, W., Xu, P., & Ren, K. (2022). Quality Assessment of Sea Surface Salinity from Multiple Ocean Reanalysis Products. *Journal of Marine Science and Engineering*, *11*(1), 54.

Wei, H.-H., Subramanian, A. C., Karnauskas, K. B., DeMott, C. A., Mazloff, M. R., & Balmaseda, M. A. (2021). Tropical pacific air-sea interaction processes and biases in CESM2 and their relation to El Niño development. *Journal of Geophysical Research, C: Oceans*, *126*(6). https://doi.org/10.1029/2020jc016967

Zeng, L., Schmitt, R. W., Li, L., Wang, Q., & Wang, D. (2019). Forecast of summer precipitation in the Yangtze River Valley based on South China Sea springtime sea surface salinity. *Climate Dynamics*, *53*(9), 5495–5509.

References from Supporting Information

O'Malley, T., Bursztein, E., Long, J., Chollet, F., Jin, H., Invernizzi, L., & Others. (2019). *KerasTuner*. https://github.com/keras-team/keras-tuner

Prusa, J., Khoshgoftaar, T. M., Dittman, D. J., & Napolitano, A. (2015). Using Random Undersampling to Alleviate Class Imbalance on Tweet Sentiment Data. *2015 IEEE International Conference on Information Reuse and Integration*, 197–202.

Geophysical Research Letters

Supporting Information for

Sea Surface Salinity Provides Subseasonal Predictability for Forecasts of Opportunity of U.S. Summertime Precipitation

Marybeth C. Arcodia[1], Elizabeth A. Barnes[1], Paul J. Durack[2], Patrick W. Keys[1], Juliette Rocha[3]

[1]Department of Atmospheric Science, Colorado State University, Fort Collins, CO, USA.

[2]Program for Climate Model Diagnosis and Intercomparison (PCMDI), Lawrence Livermore National Laboratory, Livermore, CA, USA.

[3] Department of Atmospheric Science, Texas A&M University, College Station, TX, USA.

Contents of this file

Text S1. Data Preprocessing

Daily data from 10 CESM2 ensemble members (Table S1) are used from 1850-1949 for May-August. All CESM2 data are interpolated from a 1x1 degree resolution to 2.5 x 2.5 degree resolution via bilinear interpolation for computational efficiency.

Sea surface salinity anomalies are computed via subtraction of the linear trend at each grid point of the ensemble mean for each day of the year to remove the forced response and retain only internal variability. A 3-day running average is applied to smooth the data while retaining high frequency fluctuations. Similar analyses with a 1-day and 5-day running averages of the precipitation data yielded similar results. The data are normalized by subtracting the mean and dividing by the standard deviation at each grid point.

The precipitation data are raw CESM2 data (e.g. not anomalies) averaged over the Midwest region (Fig. 1a). The daily precipitation in this region is summed cumulatively for 3 days.

Our goal is to evaluate the predictability of precipitation events across lead times spanning from the weather to subseasonal range. Therefore, we apply a Poisson weighting (Fig. S1) to the data to smooth the timeseries as lead time increases. Large weights are applied to the day being predicted for short-term forecasts (e.g. 7-day lead predictions; orange line in Fig. S1). Weights are distributed more widely as lead time increases, eventually widening into a centered nearly-Gaussian average as the upper limit of a Poisson distribution is the Gaussian distribution (e.g. 56-day lead predictions, yellow line in Fig. S1). After the precipitation time series are smoothed with the Poisson weighting (Fig. S1), the 3-day periods of precipitation are then ranked by magnitude. Periods above the 80th percentile of precipitation are classified as heavy events, designated as a 1, and the remaining 80% of the time period are classified as light events, designated as a 0. Predictions are made using the 3-day trailing average sea surface salinity map to make the prediction of the 3-day forward-cumulative sum beginning with the day of each respective lead time (0-day, 7-day, 14-day, 21-day, 28-day, 35-day, 42-day, 49-day, 56-day). For example, a 0-day lead prediction made on May 4, 1850 uses the averaged salinity input from May 1-3 to classify the precipitation event as light or heavy for May 4-7, 1850. The same input map would be used for a 7-day lead example, but to classify the precipitation event for May 11-14, 1850, and so on for all lead times. Classification is performed individually within each ensemble member for each smoothed time series based on prediction lead time.

Training of the neural networks is performed using seven ensembles with each network initialized with 5 random seeds for robustness of the results. Two members are used for validation, and one member is used for testing. The training, validation, and testing ensemble members are then randomly reselected to train another set of neural networks with 5 random seed initializations. This strategy ensures that training of networks is performed individually so that no knowledge of the test data is used in the training of the networks. This process is repeated 5 times, for a total of 25 trained neural networks (5 networks with 5 random initializations each) per lead time.

Based on the nature of the classification of the output by percentile, the training, validation, and testing data are heavily imbalanced. For effective training of the networks to learn both the light and heavy precipitation event classes, we undersample our data via randomly selecting light precipitation events to remove from the training set to balance the classes for an even 50-50 split (e.g. Prusa et al., 2015). Although 60% of the data is discarded in this process, the benefit of large ensemble climate model data used here ensures that we still have enough data

Text S2. Neural Network Architecture

The neural network architecture is depicted in the schematic in Fig. 1a. The architecture is identical for networks trained for predictions from leads of 0-35 days and then a slightly different architecture was used for leads of 42-56 days. Hyperparameter tuning was performed using the KerasTuner (O'Malley et al., 2019) to find the optimal set of parameters determined via validation accuracy. For the shorter lead forecasts, the network architecture consists of 1 hidden layer with 128 nodes with a rectified linear activation function applied (ReLU), a dropout rate of 50% and ridge regression coefficient of 0.1 to reduce overfitting, batch size of 32 samples, and a learning rate of 1.618e-5. For the longer lead forecasts beyond 35 days, the network architecture consists of 2 hidden layers with 160 and 192 nodes with a rectified linear activation function applied (ReLU) to each, a dropout rate of 80% and ridge regression coefficient of 0.01 to reduce overfitting, batch size of 32 samples, and a learning rate of 2.886e-6. All networks have a set global seed of 147483648 and are initialized with the following random seeds: 6, 26, 19, 54, 68. Networks are trained using the categorical cross-entropy loss function. Networks are trained with early stopping when the validation loss does not decrease after 25 epochs.

We note that for the lead of 7 days, the network architecture with the highest validation accuracy was slightly different than the one used here. However, the same architecture which resulted in the highest validation accuracy for leads 0, 14, 21, 28, and 35 resulted in a validation accuracy on the order of 0.001 less than the highest performing architecture. Therefore, we used the same architecture for all leads 0-35 days for simplicity.

Text S3. Water Accounting Model

The WAM2layers uses ERA5 climate reanalysis data, including hourly, 2-dimensional surface pressure, evaporation and precipitation, and hourly 3-dimensional specific humidity, and zonal and meridional winds. We use data from 2008-2021 for this analysis. We use the backtracking function of the WAM2layers, which permits the tracing of precipitated water back through the atmosphere to its origins as evaporation. In this study, we spin-up the model for six months prior to the event of interest, to ensure full saturation of the atmospheric column.

Text S4. Skill Scores

The Threat Score is a biased verification metric for categorical forecasts in which the score is based on the frequency of the event. It is defined as *hits/(hits+false alarms+misses)* in which a hit is a correctly forecasted heavy precipitation event, a false alarm is the prediction of a heavy precipitation event but it does not occur, and a miss is a prediction of a light precipitation event but a heavy event occurred. It does not account for correct rejections, e.g. correctly forecasted light events. The Gilbert Skill Score is an unbiased verification metric which accounts for the number of hits due to random chance, i.e. *chance hits*. It is defined as (*hits-chance hits)/(hits+false alarms+misses-chance hits)* where *chance hits = (hits+false alarms)*(hits+misses)/total number of forecasts*. For both skill scores, a score of zero denotes no skill, or random chance, and a skill of one is a perfect score.

Text S5. Case Studies with the WAM2layers Model

We compute the percentage of moisture that originated from a certain location for the two case studies. Specifically, we compute the amount of moisture that originated over the Caribbean Sea and Gulf of Mexico region (262-320E; 11-30N) which eventually fell in the Midwest during the event. This value is divided by the total moisture that precipitated in that region during the event. The local moisture recycling percentage is computed by the amount of moisture that originated in the analyzed region (e.g. red boxes in Fig. 4c and S5) divided by the total moisture that precipitated in that region during the event.

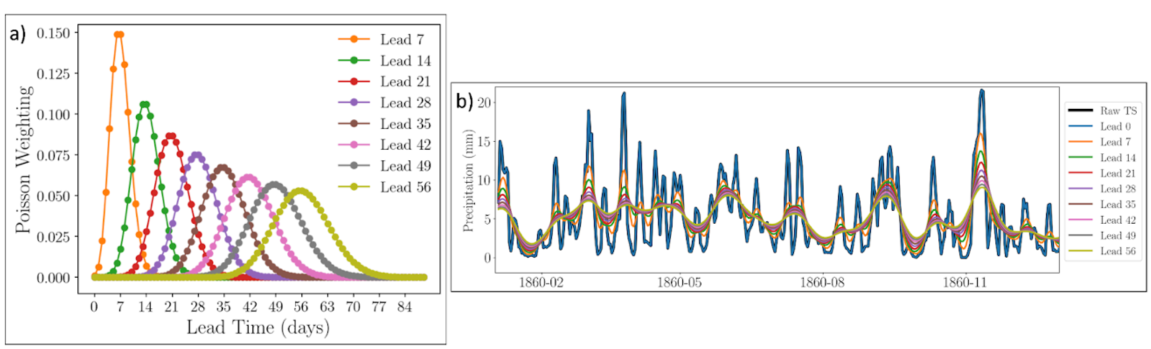

Figure S1. a) The Poisson distribution of the weights applied to the forecast period as a function of lead time. b) An example time series of the 3-day cumulative sum of precipitation in the U.S. Midwest for 1860 from ensemble member #0 showing the smoothed time series based on the Poisson weighting in (a). No weights are applied to lead of 0 days, so the raw time series (Raw TS; black line) and the time series for a lead of 0 days (Lead 0; blue line) are the same.

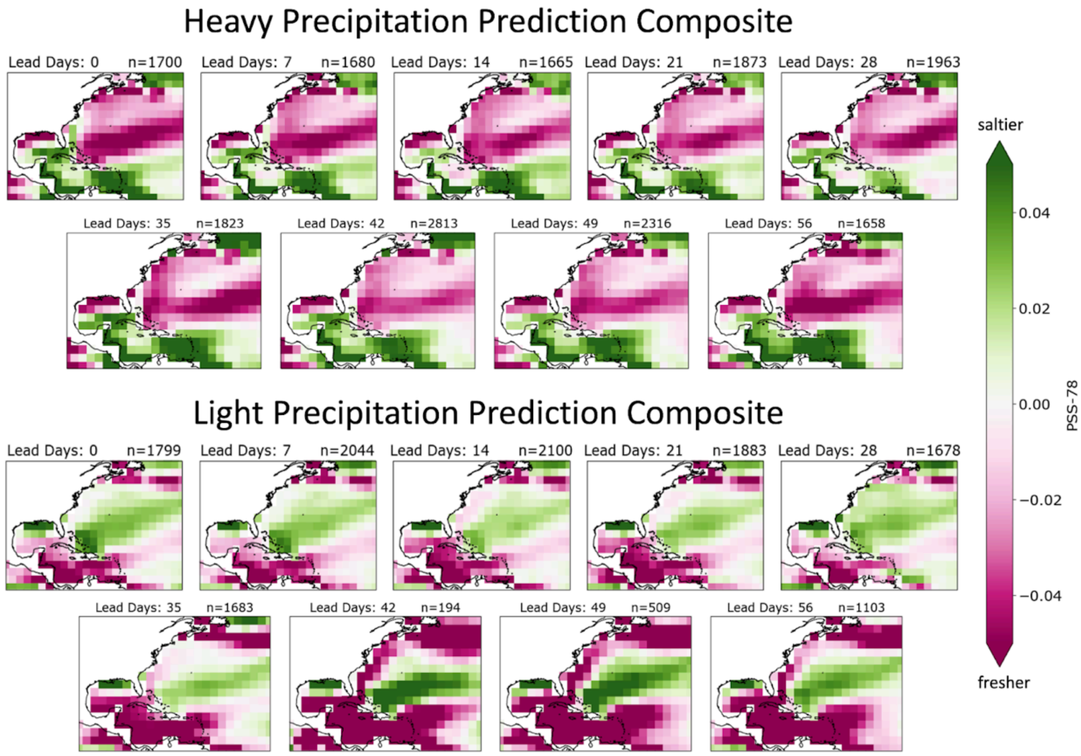

Figure S2. Composite of the sea surface salinity anomalies in PSS-78 for input maps of the 20% most confident, correct predictions for all leads for heavy predictions (top) and light predictions (bottom). Green colors represent positive sea surface salinity anomalies, or saltier waters, while pink colors represent negative sea surface salinity anomalies, or fresher waters. The number *n* represents the number of samples per composite.

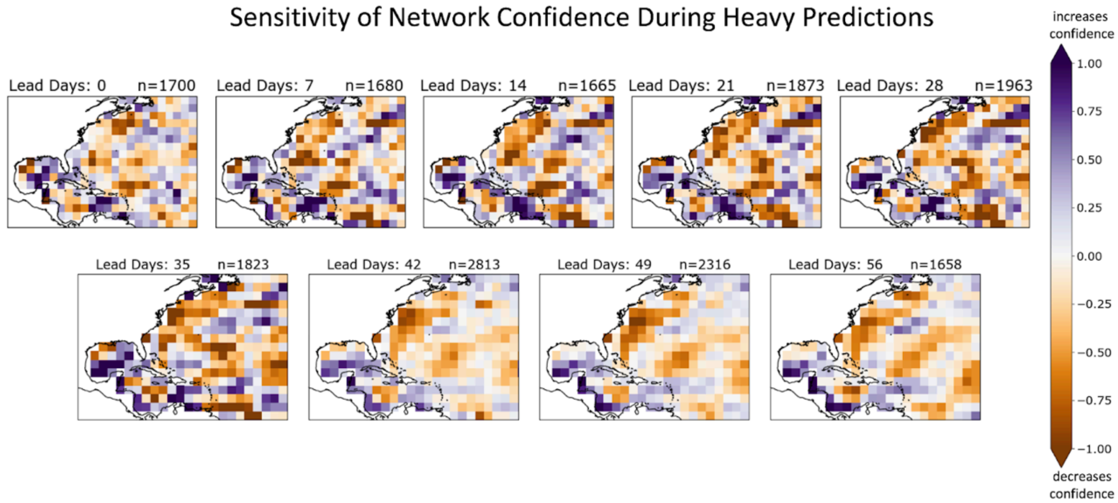

Figure S3. Saliency XAI composited heatmaps for the same days as the input maps of the 20% most confident, correct predictions for all leads for heavy predictions. Darker purple colors designate increased network confidence for positive salinity anomalies, and vice versa for orange colors. The colorbar is a unitless measure of sensitivity. The colorbar is a unitless measure of sensitivity. The number *n* represents the number of samples per composite.

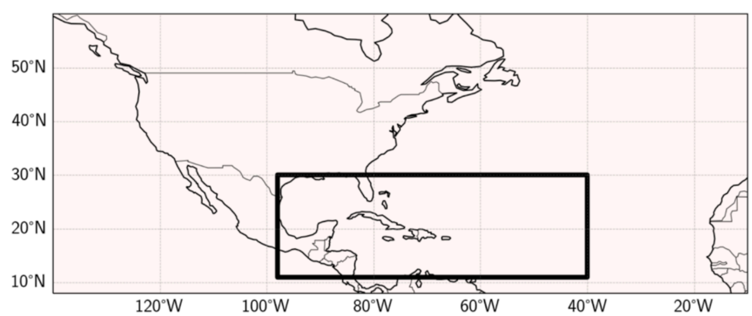

Figure S4. Region over which the moisture origin source is computed. The black box outlines 262-320E; 11-30N.

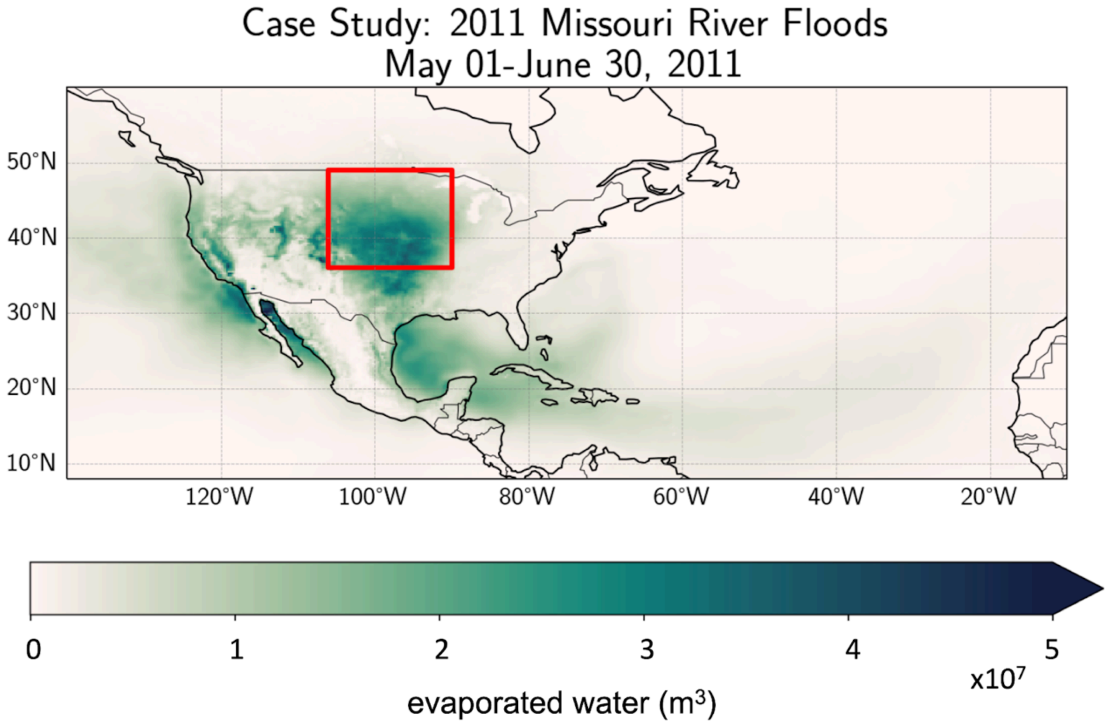

Figure S5. The sum of the evaporated water (in cubic meters) which fell as precipitation in the red boxed region computed using the WAM2layers backtracking algorithm for May 1 through June 30, 2011.

Ensemble	CESM2 Ensemble Member Name for Precipitation Variable	CESM2 Ensemble Member Name for Sea Surface Salinity Variable
0	b.e21.BHISTsmbb.f09_g17.LE2-1231.011.cam.h1.PRECT.*1850-1949*.nc	b.e21.BHISTsmbb.f09_g17.LE2-1231.011.pop.h.nday1.SSS.*1850-1949*.nc
1	b.e21.BHISTsmbb.f09_g17.LE2-1231.012.cam.h1.PRECT.*1850-1949*.nc	b.e21.BHISTsmbb.f09_g17.LE2-1231.012.pop.h.nday1.SSS.*1850-1949*.nc
2	b.e21.BHISTsmbb.f09_g17.LE2-1251.013.cam.h1.PRECT.*1850-1949*.nc	b.e21.BHISTsmbb.f09_g17.LE2-1251.013.pop.h.nday1.SSS.*1850-1949*.nc
3	b.e21.BHISTsmbb.f09_g17.LE2-1251.014.cam.h1.PRECT.*1850-1949*.nc	b.e21.BHISTsmbb.f09_g17.LE2-1251.014.pop.h.nday1.SSS.*1850-1949*.nc
4	b.e21.BHISTsmbb.f09_g17.LE2-1281.015.cam.h1.PRECT.*1850-1949*.nc	b.e21.BHISTsmbb.f09_g17.LE2-1281.015.pop.h.nday1.SSS.*1850-1949*.nc
5	b.e21.BHISTsmbb.f09_g17.LE2-1281.016.cam.h1.PRECT.*1850-1949*.nc	b.e21.BHISTsmbb.f09_g17.LE2-1281.016.pop.h.nday1.SSS.*1850-1949*.nc
6	b.e21.BHISTsmbb.f09_g17.LE2-1301.017.cam.h1.PRECT.*1850-1949*.nc	b.e21.BHISTsmbb.f09_g17.LE2-1301.017.pop.h.nday1.SSS.*1850-1949*.nc
7	b.e21.BHISTsmbb.f09_g17.LE2-1301.018.cam.h1.PRECT.*1850-1949*.nc	b.e21.BHISTsmbb.f09_g17.LE2-1301.018.pop.h.nday1.SSS.*1850-1949*.nc
8	b.e21.BHISTsmbb.f09_g17.LE2-1281.017.cam.h1.PRECT.*1850-1949*.nc	b.e21.BHISTsmbb.f09_g17.LE2-1281.017.pop.h.nday1.SSS.*1850-1949*.nc
9	b.e21.BHISTsmbb.f09_g17.LE2-1251.019.cam.h1.PRECT.*1850-1949*.nc	b.e21.BHISTsmbb.f09_g17.LE2-1251.019.pop.h.nday1.SSS.*1850-1949*.nc

Table S1. The naming convention of the ensemble members used in this study and the corresponding CESM2 ensemble member for precipitation and sea surface salinity. We used the smoothed biomass burning ensemble members (denoted by smbb). We italicize *1850-1949* because the data available are in 10-year increments. The data are downloaded then concatenated for the full time series.

Tunable Parameter	Search Space
Dropout	[0.0, 0.1, 0.2, 0.5, 0.8]
Ridge Regression (L2)	[0.01, 0.1,0.5,1.0,2.0,5.0,10.0]
# of Hidden Layers	[1,2]
# of Nodes per Layer	[32, 64, 96, 128, 160, 192, 224, 256]
Batch Size	[32, 64, 128, 256, 512]
Learning Rate	[1e-7, 1e-6, 1e-5, 1e-4, 1e-3]

Table S2. The hyperparameter search space evaluated using the KerasTuner to select the neural network architecture with the highest validation accuracy. The learning rate parameter space follows a logarithmic scale. 25 trails were performed using a random combination of the above parameters. Each network was trained for 5000 epochs with early stopping applied if validation loss increased after 25 epochs (e.g. the patience was 25).